

Multiscale Molecular Dynamics/ Hydrodynamics implementation of two dimensional ‘Mercedes Benz’ water model

Arturs Scukins^{1,a}, Dmitry Nerukh¹, Evgen Pavlov^{1,2}, Sergey Karabasov³, and Anton Markesteijn³

¹ Systems Analytics Research Institute, Aston University, Birmingham, B4 7ET, UK

² Faculty of Physics, Kiev National Taras Shevchenko University, Prospect Acad. Glushkova 4, Kiev 03127, Ukraine

³ Queen Mary University of London, Mile End Rd, London, E1 4NS, UK

Abstract. A multiscale Molecular Dynamics/Hydrodynamics implementation of the 2D Mercedes Benz (MB or BN2D) [1] water model is developed and investigated. The concept and the governing equations of multiscale coupling together with the results of the two-way coupling implementation are reported. The sensitivity of the multiscale model for obtaining macroscopic and microscopic parameters of the system, such as macroscopic density and velocity fluctuations, radial distribution and velocity autocorrelation functions of MB particles, is evaluated. Critical issues for extending the current model to large systems are discussed.

1 Introduction

In molecular modelling the focus is increasingly shifting towards large molecular systems such as biological macromolecules, the aggregates of molecules (for example various kinds of membranes, including biological), or even entire living cell organelles with all their molecular complexities (the so called ‘crowded’ biomolecular systems) [2, 3].

For example, the dynamics of proteins in water can be investigated by analysing the collective motion of particles in a liquid or biomolecular solutions. In this case glassy dynamics can be employed, where large domains consisting of water and biomolecules are found to move as a whole with very different dynamics in different domains [4]. Similarly, Umezawa et al. [5] reported that on the surface of a protein a coherent behaviour of large conglomerates of water molecules, microscopic ‘water vortices’, can be observed. It is now commonly recognised that surrounding solvent molecules play an important role in the process of protein folding [6]. Recent investigations demonstrate the connection between the water molecules dynamics in the vicinity of proteins and protein conformational motion [7]. According to the study, protein chains are guided by the water hydration shell at the periods of major conformational rearrangements. The ability to predict and control this guidance, which

^a e-mail: scukinsa@aston.ac.uk

drives protein to a particular conformation, is highly demanded because it defines all the properties and functionality of the protein.

In these processes the range of scales span several orders of magnitude. Where the small scales are needed for the atomistic description and the large scales characterise the system as a complex continuum. It is impossible to model this range of scales with a method that resolves only small, atomistic scales. At the same time, only large scales are not enough to describe the atomistic dynamics correctly. Therefore, it is necessary to use approximations in order to make two representations of the system computationally feasible. These include various coarse graining techniques, continuum modelling, combinations of the two, and other approaches.

In particular, a hybrid Molecular Dynamic/Hydrodynamics approach, which resolves both scales simultaneously, belongs to one of approximations used. In such methods the simulation domain is decomposed into the meso- and micro-scale subdomains joined by an interface. Based on the flux balance at every fixed time interval both domains receive equal but opposite mass and momentum fluxes across the hybrid interface.

Fabritis et. al. [8] showed that the mean values and fluctuations across the interface are consistent with hydrodynamics and thermodynamics, when mesoscale Landau Lifshitz Fluctuating Hydrodynamics (LL-FH) is joined with the microscale Molecular Dynamics (MD) description. Similarly, the information exchange between the domains with different representations can also be accomplished using domain decomposition techniques with a finite overlap such as Schwarz alternating method typically used for quasi-steady flow coupling. For example, [9, 10] and [11, 12] used an overlapping zone technique for coupling between MD and Hydrodynamics by ensuring the conservation of the mass and momentum fluxes through a finite size overlap region. A similar approach was used by Nie et. al. [13] to simulate Couette flow and channel flow with nanoscale rough walls. They decomposed the simulation domain into two subdomains, with a region where both subdomains overlap. In one subdomain continuum Navier-Stokes equations [14] were solved and in the other one Molecular Dynamics was used. Other popular techniques include adaptive resolution methods [15, 16, 17, 18]. With this type of methods, molecules smoothly changed their level of representation (degrees of freedom) as a function of position by moving through a transition region that connects atomistic and hydrodynamic scales.

One critical issue in using multiscale modelling is validation. To perform the validation of a system under consideration experimental data should be used or the system has to be computationally tractable at the finest scale. In the latter case, to check the validity of hydrodynamic description of a system of specific size over a specific time, which should ideally approach the hydrodynamic time scale, it first has to be modelled at atomistic resolution. Then the hydrodynamic representation of the system can be modelled and validated against the ‘ab initio’ atomistic results. The most difficult part here is that the ‘ab initio’ results are almost never available over the simulation times suitable for hydrodynamics.

Another critical issue here is the computational efficiency. This needs to answer the question if the developed multiscale method leads to significant computational savings to justify the increased model complexity. For example, in the case of the hybrid molecular dynamics/hydrodynamics methods, the following questions can be asked: did the implementation really serve its purpose to offer significant advantages in speed up in comparison with traditional single scale models such as pure molecular dynamics? If there are trade-offs associated with the speed-up versus accuracy in the multiscale simulations, what are they?

In [19] and [20], a hybrid molecular dynamics/fluctuating hydrodynamics method was developed for 2D liquid argon modelling. The idea of the approach was to use a physical analogy with two phase flow modelling, where the continuum and atomistic

representation of the same liquid were treated as the phases of a nominally two phase mixture. The governing macroscopic equations of motion of the two phase mixture were prescribed in a way to satisfy the relevant macroscopic conservation laws (mass and momentum for isothermal processes in liquids) as well as correct thermal velocity fluctuations based on the Landau-Lifshitz Fluctuating Hydrodynamics. The coupling equations naturally embed a single resolution parameter of the multiscale model. The parameter has the meaning of a partial concentration of each phase occupying the same control volume and serves to smoothly change the multiscale model resolution from fully atomistic to continuum.

In the current paper we extend the above hybrid molecular dynamics/fluctuating hydrodynamics method to water modelling at a variable resolution. For the atomistic representation of water, the so called two dimensional Mercedes Benz (BN2D) model developed by Ben-Naim [1] was used. The motivation for using the latter is driven by computational savings. Indeed, the system volume in 2D increases as L^2 in comparison to L^3 in 3D where L is the system size in each dimension. On the other hand, the system volume scales with the number of discrete particles in the system, N , which in turn, is the argument in the scaling law typical of molecular dynamics simulations that scale as $N \text{Log}(N)$ at best. Apart from the straightforward benefits of the reduced dimension in 2D, additionally, BN2D does not include computationally expensive long range Coulomb interactions that have to be calculated using methods such as Ewald summation [21, 22], which adds a large number of operations and sometimes leads to artefacts.

Thus, two dimensional water models attract interest in literature [23, 24, 25, 26, 27, 28, 29]. Such models require less computational efforts but, at the same time, they are proved to be in qualitative agreement with the experiment [30]. Detailed study of the model by Ben-Naim and other authors [23, 31, 32, 33, 34, 35] demonstrated that the model mimics real water properties. The implementation of the 2D Mercedes Benz model using MD was successfully carried out in [28, 29], where a 2D protein solution was investigated. MB water model was also used for the study of hydrophobic effects and cold denaturation [36]. Therefore, Mercedes Benz model is the next step in extending our hybrid molecular dynamics/fluctuating hydrodynamics method to more complex problem.

In comparison with our previous results for liquid argon modelling, in what follows we will investigate how well the multiscale model captures both the collective (macroscopic) and structural (microscopic) properties of water in equilibrium depending on the model resolution parameter. The results will be followed by a discussion of the critical issues that remain to be addressed in our modelling.

2 The main idea

Following the standard approach in two-phase modelling, we consider a mixture of two completely miscible liquids in the system [37]. One phase corresponds to the Lagrangian phase (MD particles) and the other is the Eulerian phase (FH continuum).

Coupling between the phases is introduced by allowing the exchange of mass and momentum between the phases. The parameter that quantifies the distribution of mass and momentum between the phases is denoted as s and mathematically it is represented by a smoothly changing function of space (and possibly time) describing the concentration of each phase. The value of s varies from 0 to 1, for example, in the centre of the system we could have mostly MD description ($s \approx 0$) and on the edges it is mostly FH ($s \approx 1$), see Fig. 1 for more explanation.

We use the following definitions. The MD phase is described by particles, the properties of which (density and velocity) are calculated as averages over the cell on

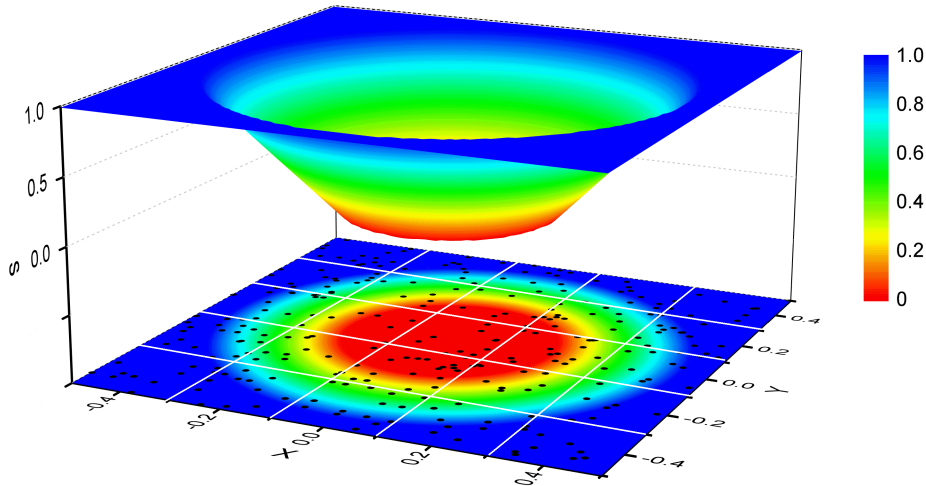


Fig. 1. In the xy -plane a 2D simulation domain is shown, with the black dots representing MD particles; the FH phase is modelled on a regular grid (white lines); the coupling parameter s has a circular symmetry profile in this example, where in the centre $s = 0$ while at the edges $s = 1$, and its projection on the xy -plane is shown in colour

the regular grid, and forms an MD ‘liquid’ with the density $\sum_p \rho_p$ and momentum $\sum_p \rho_p u_{ip}$, where $\rho_p = \frac{m_p}{V}$, u_{ip} are the MD particle’s density and velocity of the i^{th} spatial component respectively, m_p is the particle’s mass, and V is the cell volume. In this paper we use the terminology of the three-dimensional case, hence ‘volume’ is considered as area. The Eulerian phase (FH), that corresponds to the cell averages on the regular grid, forms the FH ‘liquid’ with the density ρ and the momentum ρu_i , one value of each per grid cell.

The mixture of these two liquids has the density

$$\tilde{\rho} = s\rho + (1 - s) \sum_p \rho_p \quad (1)$$

and the momentum

$$\tilde{u}_j \tilde{\rho} = s u_j \rho + (1 - s) \sum_p \rho_p u_{jp}. \quad (2)$$

Note that the summation \sum_p is done over the cell and includes the $N(t)$ particles in the cell.

We require mass and momentum conservation of the mixture of FH and MD ‘liquids’ at all concentration values s . Notably [38], in the case of liquids at isothermal conditions for which the adiabatic heat ratio approaches unity, which is the case considered here, the macroscopic conservation laws for mass and momentum are sufficient to consider because the energy equation decouples from the governing Navier-Stokes equations.

2.1 Mass conservation

The conservation laws of mass of each phase are given by:

$$\frac{\partial}{\partial t} s \rho + \frac{\partial}{\partial x_i} \tilde{u}_i s \rho = J^\rho, \quad (3)$$

$$\frac{\partial}{\partial t} (1-s) \sum_p \rho_p + \frac{\partial}{\partial x_i} (1-s) \sum_p u_{ip} \rho_p = -J^\rho, \quad (4)$$

where J^ρ is a sink/source that transfers mass between the phases, and transport velocity in (3) is the conserved velocity \tilde{u}_i , that is the average velocity of the mixture.

2.2 Momentum conservation

The FH phase is modelled using a generalisation of the deterministic Navier-Stokes equations for microscopic flows, Landau Lifshitz - Fluctuating Hydrodynamics equations [39] (LL-FH), that account for fluctuating stochastic sources originating from microscopic molecular motion.

The LL-FH model allows accurate modelling of statistical properties of the atomistic fluctuations, such as the standard deviation of mass, momentum and energy. In the limit of large volumes, the LL-FH model tends to the conventional Navier-Stokes equations.

The LL-FH equations can be efficiently solved with Eulerian methods which have reached mature state in Computational Fluid Dynamics [40] (CFD).

The momentum conservation equation for the FH ‘liquid’ can be written as

$$\frac{\partial}{\partial t} s \rho u_j + \frac{\partial}{\partial x_i} \tilde{u}_i u_j s \rho = s F_j + J^u \quad (5)$$

and for the MD ‘liquid’ it is

$$\frac{\partial}{\partial t} (1-s) \sum_p \rho_p u_{jp} + \frac{\partial}{\partial x_i} (1-s) \sum_p u_{ip} u_{jp} \rho_p = \frac{(1-s)}{V_{cell}} \sum_p F_{jp} - J^u, \quad (6)$$

where J^u is the momentum exchange rate,

$$F_j = \frac{\partial}{\partial x_i} \left(\Pi_{ij} + \tilde{\Pi}_{ij} \right), \quad (7)$$

F_j is the hydrodynamic force (per volume), V_{cell} is the cell volume, and F_{jp} is the intermolecular force that acts on each particle in the MD ‘liquid’.

As follows from [39], the deterministic hydrodynamic stress tensor is calculated as

$$\Pi_{ij} = - (P - \xi \nabla \cdot \mathbf{u}) \delta_{ij} + \eta (\partial_i u_j + \partial_j u_i - 2D^{-1} \nabla \mathbf{u} \cdot \delta_{ij}), \quad (8)$$

where $\partial_i = \frac{\partial}{\partial x_i}$, ξ and η are shear and bulk viscosities, D is the dimensionality of the system, P is pressure.

The stochastic stress tensor is calculated as

$$\tilde{\Pi}_{ij} = \sqrt{\frac{2k_B T}{\delta t \cdot V_{cell}}} \left(\sqrt{2} \sqrt{\eta} \cdot G_{ij}^s + \sqrt{D} \sqrt{\xi} \frac{tr[G]}{D} E_{ij} \right), \quad (9)$$

where k_B is the Boltzmann constant, δt is the time scale (equal to the time step in numerical implementations), T is temperature, G is the Gaussian matrix, and $G_{ij}^s = \frac{G_{ij} + G_{ij}^T}{2} - \frac{tr[G]}{D} E_{ij}$, where $tr[G]$ is the trace and E_{ij} is the unity matrix.

3 Implementation

3.1 Mass conservation

In order to maintain the conservation of mass we introduce the following dynamical law:

$$\frac{D}{Dt_0} \left(\tilde{\rho} - \sum_p \rho_p \right) = L^\rho \cdot \left(\tilde{\rho} - \sum_p \rho_p \right), \quad (10)$$

where $\frac{D}{Dt_0} = \frac{\partial}{\partial t} \cdot + \frac{\partial}{\partial x_i} \tilde{u}_i \cdot$ and L^ρ is an operator that drives the average density $\tilde{\rho}$ to the correct value $\sum_p \rho_p$ within the zone where $0 < s < 1$ and equals zero at the limits $s = 0$ and $s = 1$.

For the current implementation we used

$$L^\rho \cdot \left(\tilde{\rho} - \sum_p \rho_p \right) = \frac{\partial}{\partial x_i} \left[s(1-s) \alpha \frac{\partial}{\partial x_i} \left(\tilde{\rho} - \sum_p \rho_p \right) \right], \quad (11)$$

controlled by a parameter $\alpha > 0$.

The mass conservation equation in the form

$$\frac{\partial}{\partial t} \sum_p \rho_p + \frac{\partial}{\partial x_i} \sum_p \frac{dx_{ip}}{dt} \rho_p = 0, \quad (12)$$

yields modified velocities $\frac{dx_{ip}}{dt}$ of MD particles that include the source J^ρ .

Thus, the individual particle's velocity in the MD 'liquid' becomes

$$\frac{dx_{ip}}{dt} = u_{ip} + s(\tilde{u}_i - u_{ip}) + s(1-s)\alpha(x) \frac{1}{\rho_p N(t)} \frac{\partial}{\partial x_i} \left(\tilde{\rho} - \sum_p \rho_p \right), \quad (13)$$

where $N(t)$ is the number of particles in the cell.

For the FH 'liquid' the assumptions above yield the following mass conservation equation:

$$\frac{\partial}{\partial t} \tilde{\rho} + \frac{\partial}{\partial x_i} \tilde{u}_i \tilde{\rho} = \frac{\partial}{\partial t} \sum_p \rho_p + \frac{\partial}{\partial x_i} \tilde{u}_i \sum_p \rho_p + \frac{\partial}{\partial x_i} \left[s(1-s) \alpha \frac{\partial}{\partial x_i} \left(\tilde{\rho} - \sum_p \rho_p \right) \right]. \quad (14)$$

For detailed derivations see Appendix A.

3.2 Momentum conservation

A procedure similar to that for the mass conservation is applied to the momentum conservation.

We use

$$\frac{D}{Dt_0} \left(\tilde{u}_j \tilde{\rho} - \sum_p \rho_p u_{jp} \right) = L^u \cdot \left(\tilde{u}_j \tilde{\rho} - \sum_p \rho_p u_{jp} \right) + s F_j, \quad (15)$$

where the forcing operator is

$$L^u \cdot \left(\tilde{u}_j \tilde{\rho} - \sum_p \rho_p u_{jp} \right) = \frac{\partial}{\partial x_j} \left[s(1-s) \beta \frac{\partial}{\partial x_j} \left(\tilde{u}_j \tilde{\rho} - \sum_p \rho_p u_{jp} \right) \right], \quad (16)$$

and $\beta > 0$.

For the momentum conservation equation in the form

$$\frac{\partial}{\partial t} \sum_p \rho_p u_{jp} + \frac{\partial}{\partial x_i} \sum_p \frac{dx_{ip}}{dt} u_{jp} \rho_p - \sum_p \rho_p \frac{du_{jp}^N}{dt} = 0, \quad (17)$$

this leads to modified forces of the MD ‘liquid’, $\frac{du_{jp}^N}{dt}$, that includes the momentum exchange rate J^u .

Thus, we obtain new forces for the MD ‘liquid’:

$$\begin{aligned} \frac{du_{jp}^N}{dt} = & \frac{(1-s)}{\rho_p V_{cell}} F_{jp} + \frac{1}{\rho_p N(t)} \frac{\partial}{\partial x_i} \left[s(1-s) \alpha(x) \frac{\partial}{\partial x_i} \left(\tilde{\rho} - \sum_p \rho_p \right) \frac{\sum_p u_{jp}}{N(t)} \right] - \\ & - \frac{1}{\rho_p N(t)} \frac{\partial}{\partial x_i} \left[s(1-s) \beta(x) \frac{\partial}{\partial x_i} \left(\tilde{u}_j \tilde{\rho} - \sum_p \rho_p u_{jp} \right) \right]. \end{aligned} \quad (18)$$

For the FH liquid the following conservation equation is used:

$$\begin{aligned} \frac{\partial}{\partial t} \tilde{\rho} \tilde{u}_j + \frac{\partial}{\partial x_i} \tilde{u}_i \tilde{\rho} \tilde{u}_j = & \frac{\partial}{\partial t} \sum_p \rho_p u_{jp} + \frac{\partial}{\partial x_i} \tilde{u}_i \sum_p \rho_p u_{jp} + s F_j + \\ & + \frac{\partial}{\partial x_i} \left[s(1-s) \beta \frac{\partial}{\partial x_i} \left(\tilde{u}_j \tilde{\rho} - \sum_p \rho_p u_{jp} \right) \right]. \end{aligned} \quad (19)$$

For detailed derivations see Appendix B.

4 Simulation

The implementation can be separated into three parts: the MD simulation, the LL-FH simulation, and the coupling.

4.1 MD simulation

MB water model [1] is a simple computational model with three orientation dependent hydrogen bonding arms arranged similar to the Mercedes Benz logo, Fig. 2. Molecules interact pairwise through the Lennard-Jones term and an explicit hydrogen bonding term (which depends on the respective orientation of the arms).

The total potential is

$$\Phi = \Phi_{LJ} + \Phi_{HB}, \quad (20)$$

where the Lennard-Jones potential Φ_{LJ} is defined in the usual fashion and the summation is taken over all pairs of interacting particles

$$\Phi_{LJ} = \sum_{ij}^N 4 \epsilon_{LJ} \left(\left(\frac{\sigma_{LJ}}{r_{ij}} \right)^{12} - \left(\frac{\sigma_{LJ}}{r_{ij}} \right)^6 \right), \quad (21)$$

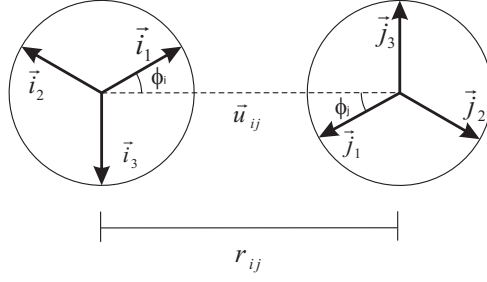


Fig. 2. Mercedes Benz model [1]

and Φ_{HB} is the explicit hydrogen bonding term defined as

$$\Phi_{HB} = \sum_{ij}^N \epsilon_{HB} \cdot G[(r_{ij} - r_{HB}), \sigma_r] \times \sum_{k,l=1}^3 G[(\mathbf{i}_k \cdot \mathbf{u}_{ij} - 1), \sigma_\phi] G[(\mathbf{j}_l \cdot \mathbf{u}_{ij} + 1), \sigma_\phi], \quad (22)$$

where G is the Gaussian function

$$G[(x), \sigma] = e^{-\frac{x^2}{2\sigma^2}}, \quad (23)$$

\mathbf{u}_{ij} is a unit vector that connects the particle centres, \mathbf{i}_k and \mathbf{j}_l are the unit vectors of the orientation of the arms, r_{ij} is the distance between the particles, the angle between a molecule's arms is 120° ; ϵ_{LJ} , ϵ_{HB} and σ_{LJ} , $\sigma_{HB} = (\sigma_r, \sigma_\phi)$ are Lennard-Jones and Mercedes Benz model well depth and contact parameters respectively. Where σ_r is used for the radial part and σ_ϕ for the angular part of the MB potential.

Because the distance between the centre and the arms of MB particle is small we assume that the external force field due to the coupling does not change at this distance. Therefore, we apply our coupling technique to the translational velocities of MB particles only.

The coupling framework yields new equations of motion, (13) and (18), for the MD simulation, that are integrated instead of the standard MD equations of motion.

The simulations are carried out in dimensionless units which can be obtained using following relationships

$$T = \frac{\epsilon_{HB}}{k_B} T^*, \quad (24)$$

$$r = r_{HB} \cdot r^*, \quad (25)$$

$$m = m_{H_2O} \cdot m^*, \quad (26)$$

$$t = \sqrt{m \cdot r_{HB}^2 / \epsilon_{HB}} \cdot t^*, \quad (27)$$

$$P \cdot V = \epsilon_{HB} \cdot P^* \cdot V^*, \quad (28)$$

where $*$ denotes the dimensionless variables. The MB model parameters are listed in Table 1. The dimensionless units can be mapped to the real ones using relationships (24) - (28) and parameters in the Table. 1.

The kinetic energy in MB model is

$$K = \sum_{i=1}^N \left(\frac{m \mathbf{v}_i^2}{2} + \frac{I \omega_i^2}{2} \right), \quad (29)$$

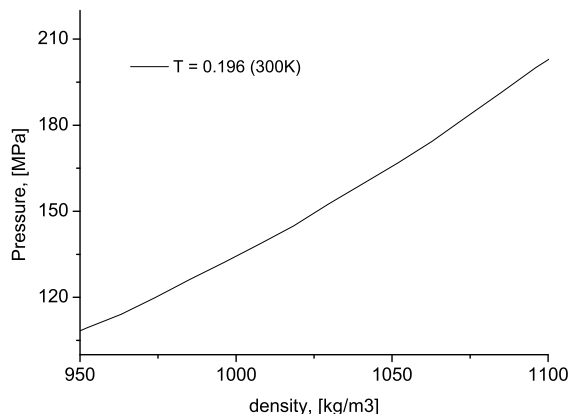


Fig. 3. Equation of state for MB water model was obtained separately from pure MB simulation

where I is the moment of inertia, \mathbf{v}_i and ω_i are the translational and angular velocities.

The equation of states (EOS), Fig. 3, was obtained from the simulations of the MB water at the temperature $T^* = 0.196$ and various densities using MD.

The dynamical properties of water are characterised by the translational (VACF) and rotational (RVACF) autocorrelation functions. The obtained autocorrelation functions, Fig. 4, coincide with the ones from 3D realistic models, such as SPC [41]. The minima on VACF and RVACF are located at approximately correct positions, which confirms the correctness of the values of the moment of inertia and mass. The moment of inertia of MB particle can be additionally adjusted such that RVACFs from SPC and MB models coincide even better.

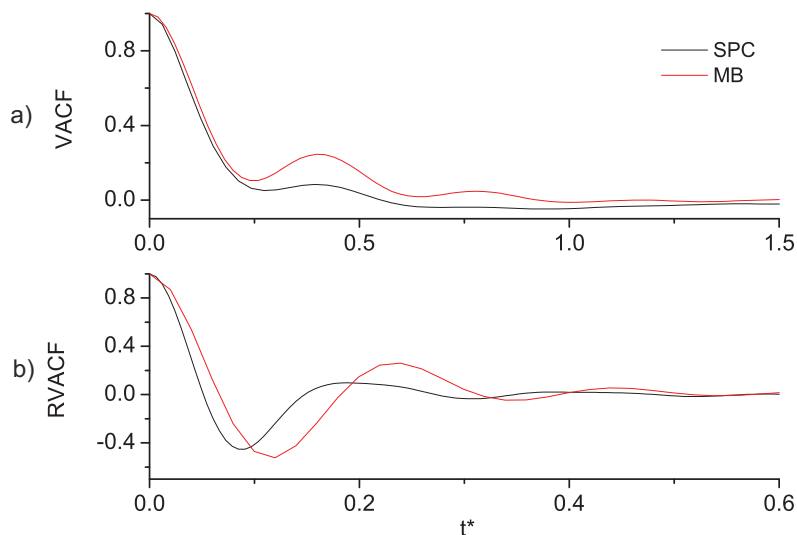


Fig. 4. a) Translational and b) rotational velocity autocorrelation functions at $T^* = 0.195$ for MB and SPC models

The structure formed by MB model, Fig. 5, is similar to the realistic water model. It also reproduces the results by Ben-Naim [1]. The maxima on RDF indicate solvation shells of different order. The maxima roughly correspond to the hexagonal ice structure of water, while a small maximum at ≈ 0.7 is formed by the ‘interstitial’ water molecules.

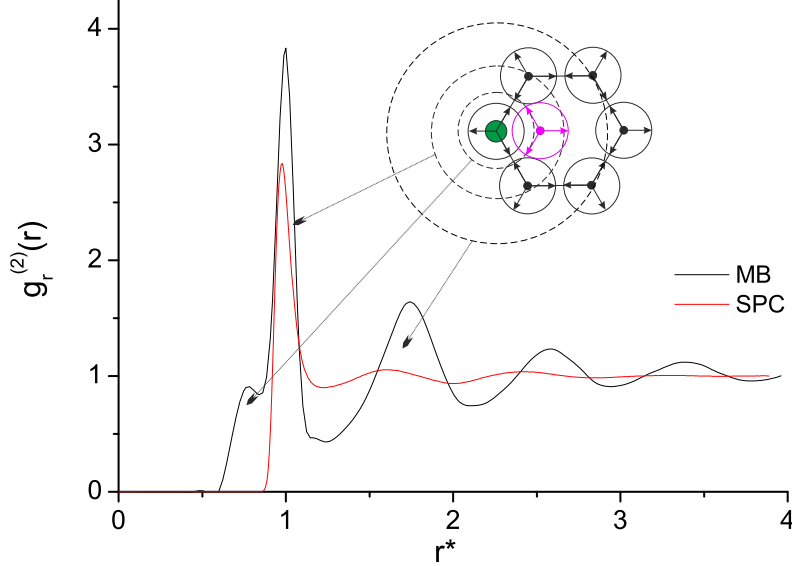


Fig. 5. Radial distribution function at $T^* = 0.16$. The reference molecule is shown in green. The ‘interstitial’ water is in magenta

The LL-FH simulation requires macroscopic transport parameters of continuum phase, such as bulk and shear viscosities, as well as the equation of state for calculating pressure, which we obtained from the separate pure MB simulations.

The commonly used method to obtain viscosities is by using the Green-Kubo relationships [42], where the bulk viscosity is calculated as an integral over time

$$\eta = \frac{V_0}{k_B T} \lim_{t \rightarrow \infty} \int_0^t B_{ACF}(t') dt', \quad (30)$$

where V_0 is the system’s volume,

$$B_{ACF}(t') = \langle \delta P(t') \delta P(0) \rangle, \quad (31)$$

and $\delta P(t) = P(t) - P_{avg}$ is the pressure fluctuations.

For the shear viscosity the following relationship was used:

$$\xi = \frac{V_0}{k_B T} \int_0^t S_{ACF}(t') dt', \quad (32)$$

where

$$S_{ACF}(t') = \langle P_{xy}(t') \cdot P_{xy}(0) \rangle. \quad (33)$$

The off-diagonal components of the pressure tensor (in the 2D case) are calculated using

$$P_{xy} = \frac{1}{V} \sum_{i=1}^N \sum_{j=i+1}^N (m \cdot u_i^x \cdot u_i^y + f_{ij}^x \cdot r_{ij}^y), \quad (34)$$

where u_i is the particle's velocity, f_{ij} is the intermolecular force, r_{ij} is the distance between the molecules and the superscripts denote x and y components.

The MB water model parameters are given in Table. 1.

Variable	Real values	Units	Dimensionless
m_{H_2O}	$18 \cdot 10^{-3}$	$\frac{kg}{mol}$	1
r_{HB}	2.78	\AA	1
ϵ_{HB}	12.742	$\frac{kJ}{mol}$	-1
ϵ_{LJ}	1.274	$\frac{kJ}{mol}$	0.1
σ_{HB}	0.25	\AA	0.085
σ_{LJ}	2.065	\AA	0.7
I	$2.938 \cdot 10^{-47}$	$kg \cdot m^2$	0.0127
k_B	$1.38 \cdot 10^{-23}$	$\frac{J}{K}$	1

Table 1. The parameters used in MD simulations [23]; r_{HB} is the hydrogen bond length, m_{H_2O} is the water molecule mass, I is the moment of inertia, ϵ_{HB} is the hydrogen bond energy, ϵ_{LJ} is the Lennard-Jones energy, σ_{LJ}^* is 0.7 of the r_{HB}^*

Simulations are conducted on a regular grid in a 2D square box split into 5 by 5 cells with 10000 MB water molecules and 25 nodes of FH values at the temperature of 300[K] and the density of $\rho = 1054 \left[\frac{kg}{m^3} \right]$.

4.2 FH simulations

The modified Fluctuating Hydrodynamics equations (14) and (19) are solved numerically with respect to the fluctuation from the cell-averaged molecular dynamics values for density and momentum as outlined in equations (62) and (63) of Appendix C. The governing partial differential equations for fluctuations (64)-(67) are discretised using a Central Leapfrog finite-difference scheme for the left hand side advection terms and central finite differences for the right hand side source terms. The total order of approximation is two in space and time. For enhanced numerical stability, a staggered formulation of the Central Leapfrog scheme is used by introducing separate variables for the cell centres and the cell faces together with a low-dissipative non-linear flux correction. Details of the staggered nonlinear Central Leapfrog scheme for advection equation as well as its implementation for the classical Landau-Lifshitz Fluctuating Hydrodynamics equations can be found in [43, 44].

4.3 Coupling

In order to implement the proposed coupling method we conduct the MD simulation using the equations (13) and (18) and the LL-FH simulation using the equations (14) and (19). Each of the simulations require information from both the MD and the LL-FH parts, thus we update/exchange the averaged in time density $\sum_p \rho_p$ and momentum $\sum_p \rho_p u_{ip}$ of the MD 'liquid' with the density $\tilde{\rho}$ and momentum $\tilde{\rho} \tilde{u}_i$ of the FH 'liquid'. The important criterium is that the time lapse in the MD and the LL-FH simulations correspond to the difference in time scales of the representations. Here

we used the ratio between the FH and MD simulations time steps $dt_{FH}/dt_{MD} = 10$, updating/exchanging the averaged over the cell values at every 10^{th} MD iteration.

The coupling parameters were chosen $\alpha, \beta = 2$, the values were selected such that the coupling strength is weak to avoid unphysical behaviour and at the same time strong enough to demonstrate the effect of coupling. Also, these parameters define the numerical stability of the simulation. The values of s have no particular importance, we used 0.1/0.5/0.8 to demonstrate the influence on the FH phase concentration in the mixture of FH and MD phases.

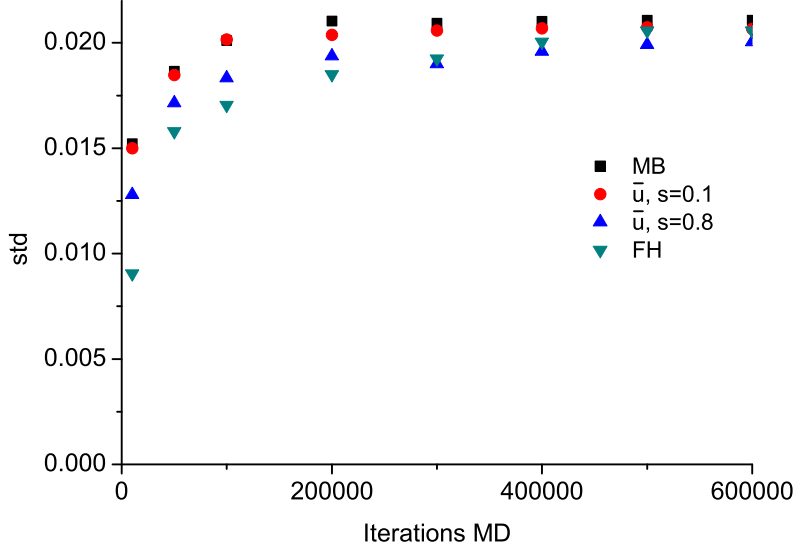


Fig. 6. Standard deviations of the average velocities (x component) of pure MB simulation, LL-FH simulation, and coupled systems

5 Results

The standard deviations (std) for the fluctuations of the average velocity \tilde{u} for the coupled systems and pure MB, LL-FH systems, Fig. 6, confirm the correctness of our scheme as they are all very similar to each other and to the correct set values. The std of \tilde{u}_x of pure MB and $s = 0.1$ on Fig. 6 are higher than the FH phase and $s = 0.8$ fluctuations. This is due to the assumption that MB water molecule is a point particle, that is not entirely true, since a molecule occupies certain ‘effective’ volume/area. That leads to the pulsations of the density and velocities, when particles migrate from one cell to another. These pulsations can be eliminated if the contributions of a molecule to the phase density and momentum is calculated as a fraction of its volume in different cells [45].

The difference between the velocity of the mixture \tilde{u}_x and the MD phase $\sum_p u_{xp}$, Fig. 7 as well as Fig. 8, shows that when $s = 0.1$ the difference is small, meaning that the velocities follow each other in both phases, while for $s = 0.8$ the difference is significantly larger and have complicated dynamics signifying the largely independent time evolution of the velocities. The effect of coupling, Fig. 7 and Fig. 8, shows that \tilde{u} inherits fluctuations of FH phase when $s \rightarrow 1$ and MD phase when $s \rightarrow 0$.

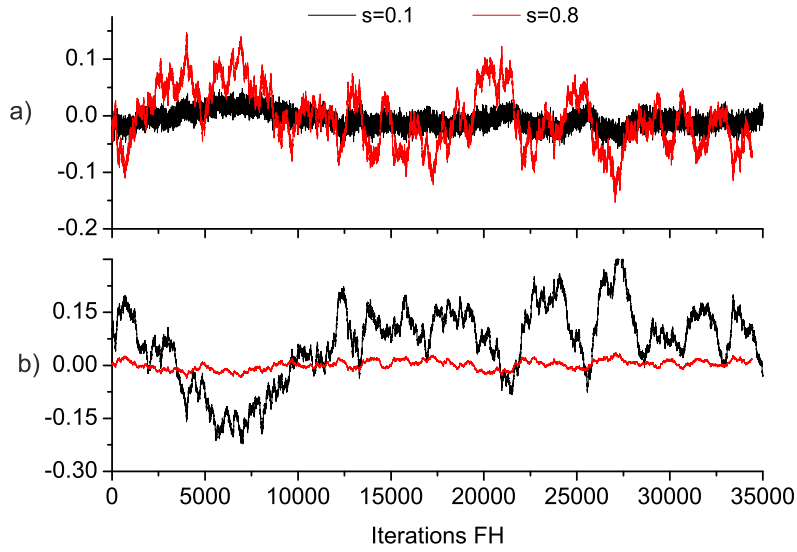


Fig. 7. The difference between the mixture and phase velocities a) $\tilde{u}_x - \sum_p u_{xp}$ and b) $\tilde{u}_x - u_x$ for $s = 0.1$ and $s = 0.8$

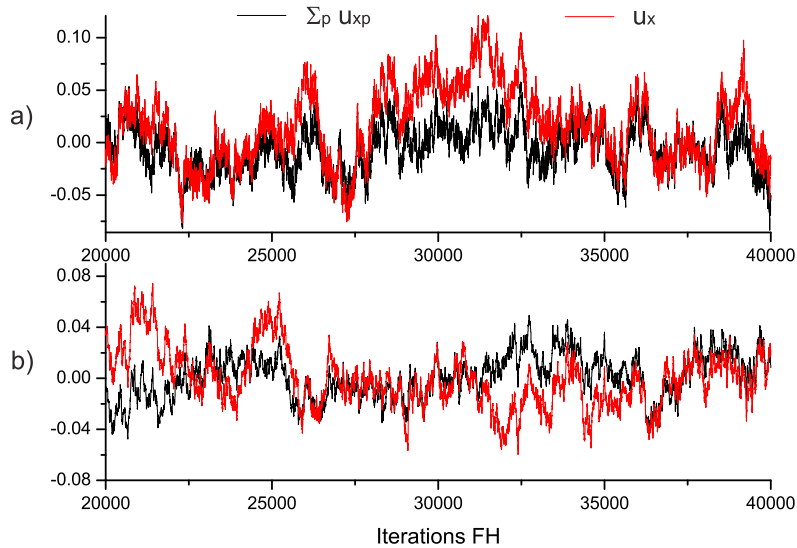


Fig. 8. Velocity x component profiles of the MD phase $\sum_p u_{xp}$ and FH phase u_x ; a) $s = 0.1$, b) $s = 0.8$

The radial distribution function of the molecules, Fig. 9, remains the same as for the MB model without coupling. This means that the external force, the ‘coupling’, does not affect the distribution of the MB molecules in the local neighbourhood.

In this paper we couple translational velocities of the MB particles with the 2D LL-FH velocities, leaving the rotational degree of freedom uncoupled. This is because in the macroscopic description it is the control-bin-averaged velocity components of the MB particles which contribute to the LL-FH conservation laws. Because of the averaging, it is the velocities of the centres of mass of each MB disk that are required

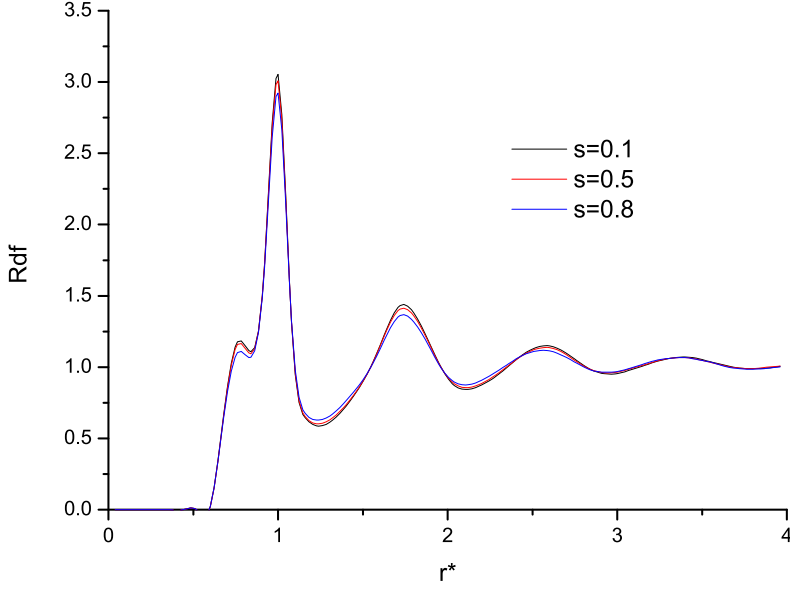


Fig. 9. Radial distribution function for different s values

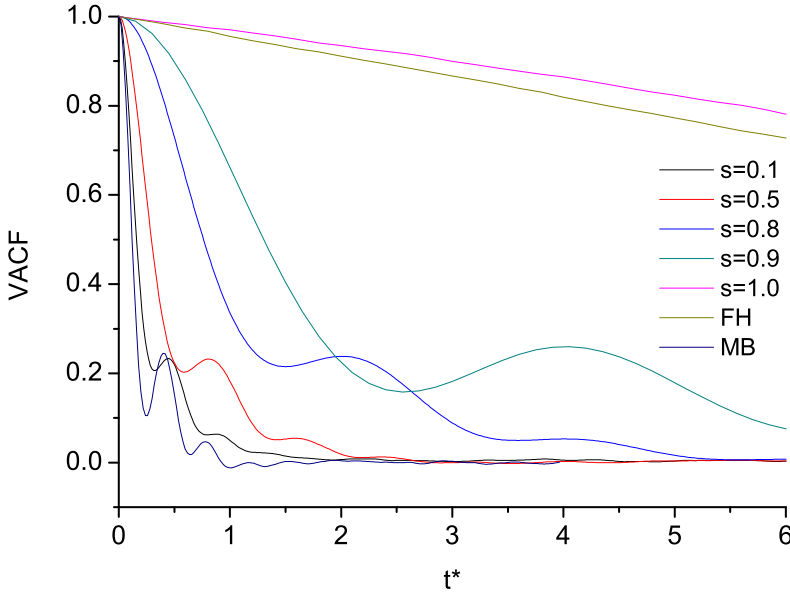


Fig. 10. Translational velocity auto-correlation function for different s values calculated from the particles velocities

to account for. The angular velocity of MB particles is only used to control angular velocity rescaling in order to maintain constant temperature of the MD particles.

The translational velocity auto-correlation function (VACF) calculated using the actual particle's velocity $\frac{dx}{dt}$, (13), is shown in Fig. 10. For larger values of s VACF becomes more stretched in time and in the limits $s \rightarrow 0$ and $s \rightarrow 1$ it approaches the corresponding VASFs of pure MD and pure FH.

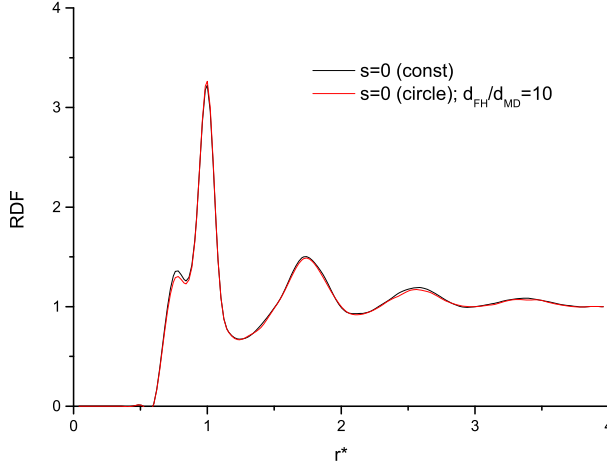


Fig. 11. Radial distribution function of the MB particles in the center of the circular shape profile of the coupling parameter 's', where $s = 0$

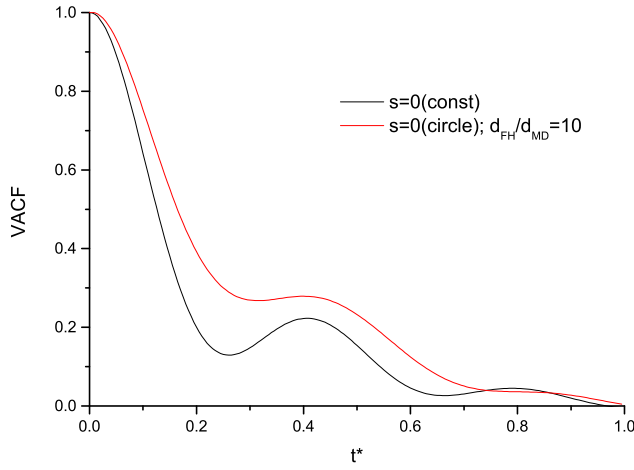


Fig. 12. Translational velocity auto-correlation function of the MB particles in the center of the profile of the coupling parameter 's', where $s = 0$

A more general case can be considered, where coupling parameter 's' changes in space:

$$s(r) = \begin{cases} S_{min}, & r < R_{MD}; \\ \frac{r-R_{MD}}{R_{HD}-R_{MD}}(S_{max} - S_{min}) + S_{min}, & R_{MD} < r < R_{HD}; \\ S_{max}, & r > R_{HD}, \end{cases}$$

where $S_{min} = 0$, $S_{max} = 0.99$, R_{MD} is 0.4 and R_{HD} is 0.9 of the simulation domain, which forms a circular shape profile of the coupling parameter 's', Fig. 1.

In the centre $s = 0$, therefore, only pure MD phase is present and at the edges $s = 0.99$, thus, FH is the main phase. The variable coupling parameter ‘s’ profile provided similar trends with respect to the magnitude of the coupling parameter ‘s’ for the statistics as well as VACF and RDF.

The RDF does not experience dramatic change regardless the value of ‘s’, Fig. 9 and Fig. 11, and correspond to the pure MB water.

In the region where ‘s’ is large VACFs are stretched along the time axis (particle’s motion becomes ‘jelly-like’) and for the small values of ‘s’ VACFs resemble pure MB. In the centre of the circle, where $s = 0$ the stretch also persists Fig. 12, although it is not as prominent as in the $s \neq 0$ zone. This is due to FH phase presence at the edges of the $s = 0$ region, that influence MB particles motion in the circle center regardless of the fact that $s = 0$.

Due to this effect the size of the circle must be considered carefully as well as the time step of the hydrodynamic part of the hybrid model so that it gradually changes in the boundary zone from MD to FH scales.

Overall it shows that the transition between the FH and MD representation is smooth and starts in the area where FH is not present (‘interface’ between MD and FH phases).

Furthermore, if the circular profile of the parameter ‘s’ is used, then MB particles close to the $s = 1$ border can stick to the FH phase and leave a vacancy in its previous position. In the region $s = 1$ MB particles do not interact between each other, hence they are dragged by the FH phase without resistance. Consequently, when MB particles stick to the FH phase collectively, empty areas appear in the region, where $s \neq 1$. Although, after certain period of time MB particles return back to the region where $s \neq 1$. This effect is not visible in the MD particles close order (RDF) analysis, since it is a macroscale effect.

6 Conclusions

A novel two way coupling scheme between Molecular Dynamics and Landau Lifshitz-Fluctuating Hydrodynamics has been extended to the Mercedes Benz water model.

In comparison with the previous work we have not only shown that the macroscopic fluctuations of the velocities and densities of one phase can be smoothly enforced on each other, but also, depending on the multiscale resolution parameter s , certain microscopic properties are preserved.

For example, the radial distribution function for MB particles is not affected by the coupling for a wide range of s . On the other hand, with the increase of the coupling parameter s , the velocity auto-correlation function (VACF) for MB particles deviates from the reference pure atomistic solution and tends to the velocity correlations in the pure FH model.

The sensitivity of the current multiscale model implementation on the coupling parameter ‘s’ was checked. It is an important step towards implementing the variable parameter ‘s’ profile as depicted in Fig. 1 with gradual reduction of the number of MD molecules when ‘s’ increases in the simulation. It is anticipated that the introduction of a variable multiscale resolution will bring essential computational benefits for modelling large systems for detailed analysis of various hydrodynamic processes, such as flows in microfluidic devices or water flows around large biomolecular aggregates, where the space-time resolution can be selected by the user or adaptively. Certainly, as discussed in the Introduction, there are several open issues on the way which remain to be solved here. One of them deals with multiple time scales concurrently in order to bridge the gap between molecular dynamics and hydrodynamics time scales. A possible solution may lie in the direction of using a relatively small MD

sub-domain surrounded by a large hybrid molecular dynamics/hydrodynamics zone, where the sub-domains of variable resolution are patched together with asynchronous time stepping. For solving unsteady fluid dynamics equations at a variable space-time resolution, asynchronous time stepping algorithms have already been proved efficient [46, 47].

7 Acknowledgement

This work has been supported in the framework of the G8 Research Councils Initiative on Multilateral Research Funding (Engineering and Physical Sciences Research Council Grant No. EP/J004308/1). DN thanks Royal Academy of Engineering and Leverhulme Trust as well as Royal Society of Chemistry for funding.

References

1. A. Ben-Naim, "Statistical mechanics of 'waterlike' particles in two dimensions. i. physical model and application of the percus-yevick equation," *J. Chem. Phys.*, vol. 54, p. 3682, 1971.
2. A. Thomas and A. Elcock, "Molecular simulations suggest protein salt bridges are uniquely suited to life at high temperatures," *J. Am. Chem. Soc.*, vol. 126, pp. 2208–2214, 2004.
3. S. McGuffee and A. Elcock, "Diffusion, crowding and protein stability in a dynamic molecular model of the bacterial cytoplasm," *PLoS Comput. Biol.*, vol. 6, p. e1000694, 2010.
4. P. Kumar, G. Franzese, S. Buldyrev, and E. Stanley, "Molecular dynamics study of orientational cooperativity in water," *Phys. Rev. E*, vol. 73, p. 041505, 2006.
5. K. Umezawa, R. Morikawa, H. Nakamura, and J. Higo, "Solvent flow patterns fluctuating largely around a protein and correlation with solvent density fluctuations: a molecular dynamics study," *J. Chem. Phys.*, vol. 132, p. 155103, 2010.
6. H. Frauenfelder, G. Chen, J. Berendzen, P. W. Fenimore, H. Jansson, B. H. McMahon, I. R. Stroe, J. Swenson, and R. D. A. Young, "Unified model of protein dynamics proc," *Natl. Acad. Sci. USA*, vol. 106, pp. 5129–5134, 2009.
7. D. Nerukh and S. Karabasov, "Water-peptide dynamics during conformational transitions," *J. Phys. Chem. Lett.*, vol. 4 (5), pp. 815–819, 2013.
8. G. D. Fabritiis, R. Delgado-Buscalioni, and P. V. Coveney, "Multiscale modelling of liquids with molecular specificity," *Phys. Rev. Lett.*, vol. 97, p. 134501, 2006.
9. S. O'Connell and P. Thompson, "Molecular dynamics-continuum hybrid computations: a tool for studying complex fluid flows," *Phys. Rev. E*, vol. 52, p. 5792, 1995.
10. E. G. Flekkoy, G. Wagner, and J. Feder, "Hybrid model for combined particle and continuum dynamics," *Europhys. Lett.*, vol. 52, p. 271276, 2000.
11. A. Asproulis, M. Kalweit, and D. Drikakis, "A hybrid molecular continuum method using point wise coupling," *Advances in Engineering Software*, vol. 46, p. 8592, 2012.
12. R. Steijl and G. Barakos, "Coupled navierstokes /molecular dynamics simulations in nonperiodic domains based on particle forcing," *Int. J. Numer. Meth. Fluids*, vol. 69, p. 13261349, 2012.
13. X. B. Nie, S. Y. Chen, W. N. E, and M. O. Robbins, "A continuum and molecular dynamics hybrid method for micro- and nano-fluid flow," *J. Fluid Mech.*, vol. 500, pp. 55–64, 2004.

14. O. Zikanov, *Essential Computational Fluid Dynamics*. New York: John Wiley, 2010.
15. S. Fritsch, S. Poblete, C. Junghans, L. Delle Site, and K. Kremer, “Adaptive resolution molecular dynamics simulation through coupling to an internal particle reservoir,” *Phys. Rev. Lett.*, vol. 108, p. 170602, 2012.
16. M. Praprotnik, L. Delle Site, and K. Kremer, “Adaptive resolution scheme (address) for efficient hybrid atomistic/mesoscale molecular dynamics simulations of dense liquids,” *Phys. Rev. E*, vol. 73, p. 066701, 2006.
17. H.Wang, C.Schuette, and L. Delle Site, “Adaptive resolution simulation (address): A smooth thermodynamic and structural transition from atomistic to coarse grained resolution and vice versa in a grand canonical fashion,” *Journal of Chemical Theory and Computation*, vol. 8, p. 2878, 2012.
18. H.Wang, C.Hartmann, C.Schuette, and L. Delle Site, “Grand-canonical-like molecular-dynamics simulations by using an adaptive-resolution technique,” *Phys. Rev. X*, vol. 3, p. 011018, 2013.
19. A. Markesteijn, S. Karabasov, A. Scukins, D. Nerukh, V. Glotov, and V. Goloviznin, “Concurrent multiscale modelling of atomistic and hydrodynamic processes in liquids,” *Philosophical Transactions of the Royal Society*, vol. A 372, p. 20130379, 2014.
20. E. Pavlov, M. Taiji, A. Scukins, A. Markesteijn, S. Karabasov, and D. Nerukh, “Visualising and controlling the flows in biomolecular systems at and between multiple scales: from atoms to hydrodynamics at different locations in time and space,” *Faraday Discussions of the Royal Society of Chemistry*, vol. DOI:10.1039/C3FD00159H, 2014.
21. M. P. Allen and D. J. Tildesley, *Computer Simulation of Liquids*. USA: Oxford University Press, 2000.
22. T. Darden, D. York, and L. Pedersen, “Particle mesh ewald: An $n \log(n)$ method for ewald sums in large systems,” *J. Chem. Phys.*, vol. 98, p. 10089, 1993.
23. K. A. T. Silverstein, A. D. J. Haymet, and K. A. Dill, “A simple model of water and the hydrophobic effect,” *J. Am. Chem. Soc.*, vol. 120, pp. 3166–3175, 1998.
24. Y. Kataoka, “Studies of liquid water by computer simulations. iii. dynamical properties of a 2d model,” *Bull. Chem. Soc. Japan*, vol. 57, pp. 1522–1527, 1983.
25. Y. Kataoka, “A molecular dynamical study of the mutual diffusion coefficient and cooperative motion in a 2-dimensional aqueous solution,” *Bull. Chem. Soc. Japan*, vol. 59, pp. 3341–3346, 1985.
26. K. Okazaki, S. Nosé, Y. Kataoka, and T. Yamamoto, “Study of liquid water by computer simulations. i. static properties of a 2d model,” *J. Chem. Phys.*, vol. 75, no. 12, pp. 5864–5874, 1981.
27. F. Hirata and P. J. Rossky, “A realization of ‘v structure’ in liquid water,” *J. Chem. Phys.*, vol. 74, pp. 6867–6874, 1981.
28. C. L. Dias, T. Ala-Nissala, M. Karttunen, I. Vattulainen, and M. Grant, “Microscopic mechanism for cold denaturation,” *Phys. Rev. Lett.*, vol. 100, p. 118101, 2008.
29. C. L. Dias, “Using microscopic mechanism for pressure and cold denaturations of proteins,” *Phys. Rev. Lett.*, vol. 109, p. 048104, 2012.
30. G. S. Kell, “Density, thermal expansivity, and compressibility of liquid water from 0 to 150 c. : Correlations and tables for atmospheric pressure and saturation reviewed and expressed on 1968 temperature scale,” *Journal Of Chemical and Engineering Data*, vol. 20, pp. 97–105, 1975.
31. T. Urbič, V. Vlady, Y. V. Kalyuzhnyi, N. T. Southall, and K. A. Dill, “A two-dimensional model of water: Solvation of nonpolar solutes,” *J. Chem. Phys.*, vol. 116, p. 723, 2002.

32. T. Urbič, V. Vlachy, Y. V. Kalyuzhnyi, and K. A. Dill, “Orientation-dependent integral equation theory for a two-dimensional model of water,” *J. Chem. Phys.*, vol. 118, p. 5516, 2003.
33. T. Urbič, V. Vlachy, Y. V. Kalyuzhnyi, and K. A. Dill, “Theory for the solvation of nonpolar solutes in water,” *J. Chem. Phys.*, vol. 127, p. 174505, 2007.
34. T. Urbič, V. Vlachy, Y. V. Kalyuzhnyi, and K. A. Dill, “An improved thermodynamic perturbation theory for mercedes-benz water,” *J. Chem. Phys.*, vol. 127, p. 174511, 2007.
35. T. Urbič and M. F. Holovkol, “Mercedesbenz water molecules near hydrophobic wall: Integral equation theories vs monte carlo simulations,” *J. Chem. Phys.*, vol. 135, p. 134706, 2011.
36. C. L. Dias, T. A.-N. J. Wong-ekkabut, I. Vattulainen, M. Grant, and M. Karttunen, “The hydrophobic effect and its role in cold denaturation,” *Cryobiology*, vol. 60, pp. 91–99, 2010.
37. D. Drew and S.L.Passman, *Theory of Multicomponent Fluids*. New York: Springer, 1999.
38. G. D. Fabritiis, M. Serrano, R. Delgado-Buscalioni, and P. Coveney, “Fluctuating hydrodynamic modeling of fluids at the nanoscale,” *Phys. Rev. E*, vol. 75, p. 026307, 2007.
39. L. Landau and E. Lifshitz, *Fluid Mechanics*. Pergamon press, 1966.
40. J. Anderson, E. Dick, G. Degrez, R. Grundmann, J. Degroote, and J. Vierendeels, *Computational Fluid Dynamics*. Berlin: Springer, 2009.
41. P. Mark and L. Nilsson, “Structure and dynamics of the tip3p, spc, and spc /e water models at 298 k,” *J. Phys. Chem. A*, vol. 105 (43), p. 99549960, 2001.
42. M. E. Tuckerman, *Statistical Mechanics: Theory and Molecular Simulation*. Oxford: Oxford University Press, 2012.
43. A. Markesteijn, S. Karabasov, V. Glotov, and V. Goloviznin, “A new non-linear two-time-level central leapfrog scheme in staggered conservation-flux variables for fluctuating hydrodynamics equations with gpu implementation,” *Computer Methods in Applied Mechanics and Engineering*, vol. under revision, 2014.
44. V. Glotov, V. Goloviznin, S. Karabasov, and A. Markesteijn, “New two level leapfrog scheme for modeling the stochastic landaulifshitz equations,” *Computational Mathematics and Mathematical Physics*, vol. 54 (2), p. 315334, 2014.
45. N. K. Voulgarakis and J.-W. Chu, “Bridging fluctuating hydrodynamics and molecular dynamics simulations of fluids,” *J. Chem. Phys.*, vol. 130, 2009.
46. A. Markesteijn and S. Karabasov, “Time asynchronous relative dimension in space method for multi-scale problems in fluid dynamics,” *J. Comp. Phys.*, vol. 258, pp. 137–164, 2014.
47. V. Semiletov and S. Karabasov, “Cabaret scheme with conservation-flux asynchronous time-stepping for nonlinear aeroacoustics problems,” *J. Comp. Phys.*, vol. 253, pp. 157–165, 2013.

Appendix A.

The mixture of FH and MD phases has the density

$$\tilde{\rho} = s\rho + (1 - s) \sum_p \rho_p \quad (35)$$

and the momentum

$$\tilde{u}_j \tilde{\rho} = s u_j \rho + (1 - s) \sum_p \rho_p u_{jp}. \quad (36)$$

Note that the \sum_p is taken over the cell and includes the $N(t)$ particles in the cell.

We require mass and momentum conservation of the mixture of FH and MD ‘liquids’ at all concentration values s .

The conservation laws of mass of each phase are given by:

$$\frac{\partial}{\partial t} s \rho + \frac{\partial}{\partial x_i} \tilde{u}_i s \rho = J^\rho, \quad (37)$$

$$\frac{\partial}{\partial t} (1-s) \sum_p \rho_p + \frac{\partial}{\partial x_i} (1-s) \sum_p u_{ip} \rho_p = -J^\rho, \quad (38)$$

where J^ρ is a sink/source that transfers mass between the phases, and transport velocity in (37) is the conserved velocity \tilde{u}_i , that is the average velocity of the mixture.

In order to maintain conservation of mass we introduce the following dynamical law:

$$\frac{D}{Dt_0} \left(\tilde{\rho} - \sum_p \rho_p \right) = L^\rho \cdot \left(\tilde{\rho} - \sum_p \rho_p \right), \quad (39)$$

where $\frac{D}{Dt_0} = \frac{\partial}{\partial t} \cdot + \frac{\partial}{\partial x_i} \tilde{u}_i \cdot$ and L^ρ is an operator that drives the corresponding deviation to the prescribed value within the zone $0 < s < 1$ and returns zero at the $s = 0$ and $s = 1$.

For the current implementation we used

$$L^\rho \cdot \left(\tilde{\rho} - \sum_p \rho_p \right) = \frac{\partial}{\partial x_i} \left[s (1-s) \alpha \frac{\partial}{\partial x_i} \left(\tilde{\rho} - \sum_p \rho_p \right) \right], \quad (40)$$

controlled by a parameter $\alpha > 0$.

Eq.(39) can be rewritten as

$$\frac{\partial}{\partial t} \left(\tilde{\rho} - \sum_p \rho_p \right) + \frac{\partial}{\partial x_i} \tilde{u}_i \left(\tilde{\rho} - \sum_p \rho_p \right) = \frac{\partial}{\partial x_i} \left[s (1-s) \alpha \frac{\partial}{\partial x_i} \left(\tilde{\rho} - \sum_p \rho_p \right) \right], \quad (41)$$

and substituting $\tilde{\rho}$ in equation above we obtain density difference between FH and MD phases:

$$\frac{\partial}{\partial t} s \left(\rho - \sum_p \rho_p \right) + \frac{\partial}{\partial x_i} \tilde{u}_i s \left(\rho - \sum_p \rho_p \right) = \frac{\partial}{\partial x_i} \left[s (1-s) \alpha \frac{\partial}{\partial x_i} \left(\tilde{\rho} - \sum_p \rho_p \right) \right]. \quad (42)$$

In the eq.(42) we collect terms to express J^ρ explicitly according to the eq.(37)

$$J^\rho = \frac{\partial}{\partial t} s \sum_p \rho_p + \frac{\partial}{\partial x_i} \tilde{u}_i s \sum_p \rho_p + \frac{\partial}{\partial x_i} \left[s (1-s) \alpha \frac{\partial}{\partial x_i} \left(\tilde{\rho} - \sum_p \rho_p \right) \right] \quad (43)$$

Substitution of the J^ρ in the eq.(38) yields

$$\begin{aligned} \frac{\partial}{\partial t}(1-s) \sum_p \rho_p + \frac{\partial}{\partial x_i}(1-s) \sum_p \rho_p u_{ip} &= -\frac{\partial}{\partial t} s \sum_p \rho_p - \frac{\partial}{\partial x_i} \tilde{u}_i s \sum_p \rho_p - \\ & - \frac{\partial}{\partial x_i} \left[s(1-s) \alpha \frac{\partial}{\partial x_i} \left(\tilde{\rho} - \sum_p \rho_p \right) \right], \end{aligned} \quad (44)$$

that can be simplified to

$$\begin{aligned} \frac{\partial}{\partial t} \sum_p \rho_p + \frac{\partial}{\partial x_i} s \tilde{u}_i \sum_p \rho_p + \frac{\partial}{\partial x_i}(1-s) \sum_p \rho_p u_{ip} &= \\ = -\frac{\partial}{\partial x_i} \left[s(1-s) \alpha \frac{\partial}{\partial x_i} \left(\tilde{\rho} - \sum_p \rho_p \right) \right], \end{aligned} \quad (45)$$

The mass conservation equations in the form

$$\frac{\partial}{\partial t} \sum_p \rho_p + \frac{\partial}{\partial x_i} \sum_p \frac{dx_{ip}}{dt} \rho_p = 0. \quad (46)$$

yields modified velocities $\frac{dx_{ip}}{dt}$ of MD particles that include the source J^p .

Combining eq.(46) with eq.(45) yields

$$\begin{aligned} -\frac{\partial}{\partial x_i} \sum_p \frac{dx_{ip}}{dt} \rho_p + \frac{\partial}{\partial x_i} \tilde{u}_i \sum_p \rho_p + \frac{\partial}{\partial x_i}(1-s) \sum_p \rho_p u_{ip} &= \\ = -\frac{\partial}{\partial x_i} \left[s(1-s) \alpha \frac{\partial}{\partial x_i} \left(\tilde{\rho} - \sum_p \rho_p \right) \right]. \end{aligned} \quad (47)$$

Integrating once the equation above we get

$$\sum_p \frac{dx_{ip}}{dt} \rho_p = \tilde{u}_i \sum_p \rho_p + (1-s) \sum_p \rho_p u_{ip} + \left[s(1-s) \alpha \frac{\partial}{\partial x_i} \left(\tilde{\rho} - \sum_p \rho_p \right) \right], \quad (48)$$

for each particle in the cell we have

$$\frac{dx_{ip}}{dt} = u_{ip} + s(\tilde{u}_i - u_{ip}) + s(1-s)\alpha(x) \frac{1}{\rho_p N(t)} \frac{\partial}{\partial x_i} \left(\tilde{\rho} - \sum_p \rho_p \right), \quad (49)$$

where $N(t)$ is a number of particles in the cell.

Appendix B.

A procedure similar to that for the mass conservation is applied to the momentum conservation.

For the FH ‘liquid’ we use following momentum conservation equation

$$\frac{\partial}{\partial t} s \rho u_j + \frac{\partial}{\partial x_i} \tilde{u}_i u_j s \rho = s F_j + J^u, \quad (50)$$

and for MD ‘liquid’

$$\frac{\partial}{\partial t} (1-s) \sum_p \rho_p u_{jp} + \frac{\partial}{\partial x_i} (1-s) \sum_p u_{ip} u_{jp} \rho_p = \frac{(1-s)}{V_{\text{cell}}} \sum_p F_{jp} - J^u. \quad (51)$$

In order to maintain momentum conservation we introduce the following dynamical law:

$$\frac{D}{Dt_0} \left(\tilde{u}_j \tilde{\rho} - \sum_p \rho_p u_{jp} \right) = L^u \cdot \left(\tilde{u}_j \tilde{\rho} - \sum_p \rho_p u_{jp} \right) + s F_j, \quad (52)$$

where the forcing operator is

$$L^u \cdot \left(\tilde{u}_j \tilde{\rho} - \sum_p \rho_p u_{jp} \right) = \frac{\partial}{\partial x_j} \left[s(1-s) \beta \frac{\partial}{\partial x_j} \left(\tilde{u}_j \tilde{\rho} - \sum_p \rho_p u_{jp} \right) \right], \quad (53)$$

and $\beta > 0$.

Expanding eq.(52) we get:

$$\begin{aligned} \frac{\partial}{\partial t} \left(\tilde{u}_j \tilde{\rho} - \sum_p \rho_p u_{jp} \right) + \frac{\partial}{\partial x_i} \tilde{u}_i \left(\tilde{u}_j \tilde{\rho} - \sum_p \rho_p u_{jp} \right) &= s F_j + \\ + \frac{\partial}{\partial x_j} \left[s(1-s) \beta \frac{\partial}{\partial x_j} \left(\tilde{u}_j \tilde{\rho} - \sum_p \rho_p u_{jp} \right) \right], \end{aligned} \quad (54)$$

where $\tilde{u}_i \tilde{\rho}$ can be replaced with eq.(36) yielding

$$\begin{aligned} \frac{\partial}{\partial t} s \left(u_j \rho - \sum_p \rho_p u_{jp} \right) + \frac{\partial}{\partial x_i} s \tilde{u}_i \left(u_j \rho - \sum_p \rho_p u_{jp} \right) &= s F_j + \\ + \frac{\partial}{\partial x_j} \left[s(1-s) \beta \frac{\partial}{\partial x_j} \left(\tilde{u}_j \tilde{\rho} - \sum_p \rho_p u_{jp} \right) \right] \end{aligned} \quad (55)$$

In the eq.(55) we collect terms to express J^u explicitly according to the eq.(50)

$$J^u = \frac{\partial}{\partial t} s \sum_p \rho_p u_{jp} + \frac{\partial}{\partial x_i} s \tilde{u}_i \sum_p \rho_p u_{jp} + \frac{\partial}{\partial x_j} \left[s(1-s) \beta \frac{\partial}{\partial x_j} \left(\tilde{u}_j \tilde{\rho} - \sum_p \rho_p u_{jp} \right) \right] \quad (56)$$

When the momentum exchange rate J^u is known it can be substituted in the momentum conservation equation for MD eq.(51)

$$\begin{aligned} \frac{\partial}{\partial t} \sum_p \rho_p u_{jp} + \frac{\partial}{\partial x_i} (1-s) \sum_p u_{ip} u_{jp} \rho_p &= \frac{(1-s)}{V_{\text{cell}}} \sum_p F_{jp} - \frac{\partial}{\partial x_i} s \tilde{u}_i \sum_p \rho_p u_{jp} - \\ - \frac{\partial}{\partial x_j} \left[s(1-s) \beta \frac{\partial}{\partial x_j} \left(\tilde{u}_j \tilde{\rho} - \sum_p \rho_p u_{jp} \right) \right]. \end{aligned} \quad (57)$$

For the momentum conservation equation in the form

$$\frac{\partial}{\partial t} \sum_p \rho_p u_{jp} + \frac{\partial}{\partial x_i} \sum_p \frac{dx_{ip}}{dt} u_{jp} \rho_p = \sum_p \rho_p \frac{du_{jp}^N}{dt}, \quad (58)$$

this leads to the modified forces of the MD ‘liquid’ $\frac{du_{jp}^N}{dt}$, that includes the momentum exchange rate J^u .

Eq.(58) and eq.(57) yields

$$\begin{aligned} \frac{\partial}{\partial x_i} \sum_p \frac{dx_{ip}}{dt} u_{jp} \rho_p &= \frac{\partial}{\partial x_i} s \tilde{u}_i \sum_p u_{jp} \rho_p + \\ + \frac{\partial}{\partial x_i} (1-s) \sum_p u_{jp} \rho_p u_{ip} &+ \frac{\partial}{\partial x_i} \left[s(1-s) \alpha \frac{\partial}{\partial x_i} \left(\tilde{\rho} - \sum_p \rho_p \right) \right] \frac{\sum_p u_{jp}}{N(t)}, \end{aligned} \quad (59)$$

the modified force/acceleration acting on the particles in the cell is:

$$\begin{aligned} \sum_p \rho_p \frac{du_{jp}^N}{dt} &= \frac{(1-s)}{V_{cell}} \sum_p F_{jp} + \\ + \frac{\partial}{\partial x_i} \left[s(1-s) \alpha \frac{\partial}{\partial x_i} \left(\tilde{\rho} - \sum_p \rho_p \right) \right] \frac{\sum_p u_{jp}}{N(t)} &- \frac{\partial}{\partial x_j} \left[s(1-s) \beta \frac{\partial}{\partial x_j} \left(\tilde{u}_j \tilde{\rho} - \sum_p \rho_p u_{jp} \right) \right]. \end{aligned} \quad (60)$$

For the individual particles we get

$$\begin{aligned} \frac{du_{jp}^N}{dt} &= \frac{(1-s)}{\rho_p V_{cell}} F_{jp} + \frac{1}{\rho_p N(t)} \frac{\partial}{\partial x_i} \left[s(1-s) \alpha(x) \frac{\partial}{\partial x_i} \left(\tilde{\rho} - \sum_p \rho_p \right) \right] \frac{\sum_p u_{jp}}{N(t)} - \\ - \frac{1}{\rho_p N(t)} \frac{\partial}{\partial x_i} \left[s(1-s) \beta(x) \frac{\partial}{\partial x_i} \left(\tilde{u}_j \tilde{\rho} - \sum_p \rho_p u_{jp} \right) \right]. \end{aligned} \quad (61)$$

Appendix C

By introducing new variables

$$\rho' = \tilde{\rho} - \sum_p \rho_p, \quad (62)$$

$$u' \rho' = \tilde{u}_j \tilde{\rho} - \sum_p \rho_p u_{jp} \quad (63)$$

the LL-FH equations can be written as:

$$\frac{\partial}{\partial t} \rho' + \frac{\partial}{\partial x_i} \tilde{u}_i \rho' = Q_\rho, \quad (64)$$

where

$$Q_\rho = \frac{\partial}{\partial x_i} \left[s(1-s) \alpha \frac{\partial}{\partial x_i} (\rho') \right] \quad (65)$$

and

$$\frac{\partial}{\partial t} u'_j \rho' + \frac{\partial}{\partial x_i} \tilde{u}_i u'_j \rho' = s F_j + Q_u, \quad (66)$$

where

$$Q_u = \frac{\partial}{\partial x_j} \left[s(1-s) \beta \frac{\partial}{\partial x_j} (u'_j \rho') \right]. \quad (67)$$

The pure FH force is used from the classic LL-FH framework

$$F_j = \frac{\partial}{\partial x_i} \left(\Pi_{ij} + \tilde{\Pi}_{ij} \right), \quad (68)$$

where the stress tensor is calculated as

$$\Pi_{ij} = - (p - \xi \nabla \cdot \mathbf{u}) \delta_{ij} + \eta (\partial_i u_j + \partial_j u_i - 2D^{-1} \nabla \mathbf{u} \cdot \delta_{ij}), \quad (69)$$

and the stochastic stress tensor as

$$\tilde{\Pi}_{ij} = \sqrt{\frac{2k_B T}{\delta t \cdot V_{cell}}} \left(\sqrt{2} \sqrt{\eta} \cdot G_{ij}^s + \sqrt{D} \sqrt{\xi} \frac{tr[G]}{D} E_{ij} \right) \quad (70)$$

where $\partial_i = \frac{\partial}{\partial x_i}$ and G is the Gaussian matrix, $G_{ij}^s = \frac{G_{ij} + G_{ij}^T}{2} - \frac{tr[G]}{D} E_{ij}$, E_{ij} is the unity matrix and $tr[\]$ stands for the matrix trace.

The LL-FH equations are solved with a second-order centered finite-difference scheme based on the characteristic decomposition.